



MOX-Report No. 38/2018

**Prediction of long term restenosis risk after surgery in  
the carotid bifurcation by hemodynamic and geometric  
analysis**

Domanin, M.; Gallo, D.; Vergara, C.; Biondetti, P.; Forzenigo,  
L.V.; Morbiducci, U.

MOX, Dipartimento di Matematica  
Politecnico di Milano, Via Bonardi 9 - 20133 Milano (Italy)

[mox-dmat@polimi.it](mailto:mox-dmat@polimi.it)

<http://mox.polimi.it>

1 **PREDICTION OF LONG TERM RESTENOSIS RISK AFTER SURGERY IN THE CAROTID**  
2 **BIFURCATION BY HEMODYNAMIC AND GEOMETRIC ANALYSIS**

3

4 M. Domanin <sup>a-b \*</sup>, D. Gallo <sup>c \*</sup>, C. Vergara <sup>d</sup>, P. Biondetti <sup>e</sup>, L.V. Forzenigo <sup>e</sup>, U. Morbiducci <sup>c</sup>

5

6 a Department of Clinical Sciences and Community Health, Università di Milano, Italy

7 b Unità Operativa di Chirurgia Vascolare, Fondazione I.R.C.C.S. Cà Granda Ospedale Maggiore  
8 Policlinico, Milano, Italy,

9 c PolitoBIOMed Lab, Department of Mechanical and Aerospace Engineering, Politecnico di  
10 Torino, Turin, Italy;

11 d MOX, Dipartimento di Matematica, Politecnico di Milano, Italy.

12 e Unità Operativa di Radiologia, Fondazione I.R.C.C.S. Cà Granda Ospedale Maggiore Policlinico,  
13 Milano, Italy,

14

15 \* The authors equally contributed to this study

16

17 maurizio.domanin@unimi.it Corresponding author

18 diego.gallo@polito.it

19 umberto.morbiducci@polito.it

20 christian.vergara@polimi.it

21 lvforzenigo@gmail.com

22 biondetti.pietrorai@gmail.com

23

24 **Short title:** HEMODYNAMIC AND GEOMETRIC RESTENOSIS RISK IN CAROTID

25

26 **Disclosure** The authors have no personal, financial, or institutional interest in any of the drugs,  
27 materials, or devices described in this article.

28

29

1 **ABSTRACT**

2

3 **Objective-** Carotid restenosis is a common complication occurring after carotid endarterectomy  
4 (CEA). This study aimed to explore the potential of local hemodynamic disturbances and carotid  
5 bifurcation geometry to predict long-term restenosis at 60 months after CEA.

6 **Methods-** Thirteen carotid bifurcations with a stenosis greater than 70% were submitted to CEA.  
7 Arteriotomy repair was performed with patch graft (PG) angioplasty in 9 cases, with primary  
8 closure (PC) in 4 cases. MRI acquisitions were performed within a month after surgery for  
9 hemodynamic and geometric characterization. Personalized computational fluid dynamic  
10 simulations were performed and hemodynamic disturbances were quantified in terms of  
11 exposure to low and oscillatory wall shear stress (WSS). Each carotid geometry was characterized  
12 automatically in terms of flare (i.e., the expansion at the carotid bulb) and tortuosity proximal to  
13 the bifurcation. Based on hemodynamics and geometry, cases were classified into three categories  
14 of “geometric” or “hemodynamic” restenosis risk. At 60 months after CEA, eligible participants  
15 underwent duplex ultrasound scan and peak systolic velocity measurement for the detection of  
16 restenosis, with extraction of intima-media thickness from five selected locations along the carotid  
17 bifurcation.

18 **Results-** More unfavorable hemodynamic conditions established in PG than PC cases. Carotid flare  
19 was found to be significantly associated with the exposure to low WSS and therefore considered  
20 to define the geometric restenosis risk. No significant associations were found for tortuosity. The  
21 two cases characterized by the highest flare and the largest exposure to low WSS developed  
22 restenosis >50% at 60 months. A high correspondence was found between morphological DUS  
23 observations of myointimal thickening or new atheroma development and low and oscillatory  
24 WSS regions.

25 **Conclusions-** The quantitative analysis of hemodynamics and geometry holds potential for the  
26 stratification of patients at risk for development of late restenosis after CEA. Moreover, it can help  
27 the understanding of the mechanistic processes underlying restenosis development, potentially  
28 guiding the clinical decision between PG vs. PC. Our findings suggest that arteriotomy repair  
29 should avoid an artificial flare, that is linked with restenosis via the generation of flow

1 disturbances. Geometric characterization from imaging data is a convenient, fast and easy method  
2 that can be integrated in the clinical practice.

3  
4 **Keywords:** Cerebrovascular, Carotid pathophysiology, endarterectomy, recurrent stenosis,  
5 computational fluid dynamics, Wall shear stress

## 11 INTRODUCTION

13 Restenosis, i.e. the recurrence of narrowing of the arterial lumen at the same site of the previous  
14 carotid endarterectomy (CEA), is an important complication affecting CEA outcome. Its overall  
15 incidence is 5.8%, with 8.0% of symptomatic patients.<sup>1-2</sup> In the first two years after surgery, when  
16 the risk for restenosis is higher,<sup>3-4</sup> restenosis is usually intended as development of myointimal  
17 hyperplasia, while intermediate (2 to 5 years) and late (>5 years) restenosis are deemed similar  
18 to primary atherosclerotic lesions.<sup>5</sup>

19 To minimize the risk of narrowing of the arterial lumen, the use of patch grafts (PG) for the closure  
20 of the longitudinal arteriotomy has been proposed as an alternative to primary closure (PC).  
21 Notwithstanding the recommendation for routinary use of PG by current guidelines,<sup>6-7</sup> doubts  
22 have been raised over its effectiveness. In fact, on one hand PG insertion lowers the restenosis risk  
23 in the early postoperative period, when PC technical defect might result in lumen narrowing.<sup>1</sup> On  
24 the other hand, PG involves longer cross-clamping time,<sup>8</sup> association of neurocognitive deficits<sup>9</sup>  
25 and higher risk of infection or pseudoaneurysm development.<sup>10</sup> A selective use for PG based on  
26 gender or on the measure of carotid diameters has also been suggested.<sup>11</sup> However, although the  
27 clinically convenient geometric measurement of the carotid diameter could be helpful for practical  
28 purposes, it could result in an oversimplification of the decision criteria.

1 Reliable decision criteria should be based on the understanding of the mechanistic processes  
2 underlying restenosis development. Among several factors, local hemodynamic disturbances are  
3 thought to contribute to the development of late restenosis after CEA.<sup>12</sup> This is supported by  
4 several evidences proving a key role of wall shear stress (WSS), i.e. the tangential friction stress  
5 exerted by the flowing blood on the endothelial cells lining the vessel lumen.<sup>13</sup> In particular, WSS  
6 having low average magnitude and large oscillatory (directional) changes contributes to  
7 atherosclerosis development at the carotid bulb.<sup>13-14</sup> Currently, WSS is most reliably assessed  
8 through image-based computational fluid dynamics (CFD). As an integration, or even an  
9 alternative, to CFD-based WSS estimation, previous studies proposed specific geometric attributes  
10 of the carotid bifurcation as surrogate markers of the burden of low and oscillatory WSS.<sup>15-17</sup>  
11 In the present study, we aim to establish whether the post-CEA hemodynamics and geometry can  
12 predict the risk of late restenosis development. In detail, in a cohort of 13 carotid bifurcations  
13 submitted to CEA with two different closure techniques (PG and PC), firstly image-based  
14 computational hemodynamic simulations were performed to explore the potential of low and  
15 oscillatory WSS to predict late clinical outcomes at 60 months. Secondly, geometric attributes of  
16 the carotid bifurcation predicting WSS disturbances were selected and linked to late restenosis, in  
17 an effort to define mechanistic-based criteria that can be easily translated into the clinical practice  
18 to guide the choice between PG vs. PC.

19

## 20 **METHODS**

21

### 22 **Ethics Statement**

23 The study has been approved by the I.R.C.C.S. Fondazione Policlinico Ethics Committee according  
24 to institutional ethics guidelines. All the patients gave their signed consent for the publication of  
25 data.

26

### 27 **Patient population data**

28 Thirteen consecutive carotid bifurcations with a stenosis >70% were submitted to CEA in 12  
29 patients. All cases were asymptomatic, one case (8.3%) had contralateral occlusion of the internal

1 carotid artery (ICA) and three cases (25.0%) have been previously submitted to contralateral CEA.  
2 Ages, gender, localizations of carotid blockage, diameters of ICA and closure techniques, are listed  
3 in Table I. All CEAs were performed under regional block anesthesia.  
4 PG angioplasty was performed in 9 cases (PG1-9) using 6x75mm polyester collagen-coated patch  
5 (Ultra-thin Intervascular®, Mahwah, U.S.A), tailored and distally trimmed to give a smoothly  
6 tapered transition. Cases PG1 and PG2 (right and left carotid in the same patient, respectively)  
7 were submitted to obliged PG according to guidelines, while in remaining cases PG was preferred  
8 to PC since ICA diameter was lower than 5.0 mm.  
9 PC was the first choice in three cases (PC1, PC3, PC4) for lesions limited to the carotid bulb (CB)  
10 or with ICA diameter  $\geq 5.0$  mm. For case PC2, initially scheduled for PG, we adopted PC for  
11 intraoperative lack of patient's collaboration in absence of major neurological concerns.  
12 All the patients were then submitted to duplex ultrasound scan (DUS) follow-up at 3, 24 and 60  
13 months and velocities are all reported in Table II. In case DUS results showed  $>50\%$  stenosis by  
14 the European Carotid Stenosis Trial (ECST) standard, or a peak systolic velocity (PSV) of  $>130$   
15 cm/s,<sup>18</sup> magnetic resonance angiography (MRA) was conducted. Cases exhibiting  $>50\%$  stenosis  
16 on the MRA examinations by the North American Symptomatic Carotid Endarterectomy Trial  
17 (NASCET) standard were defined as cases of restenosis. Follow-ups at 3 and 24 months resulted  
18 negative to the detection of restenosis. During the follow-up period, two patients died respectively  
19 for myocardial infarction (PG4), and pancreatic carcinoma (PG8) at 36 months. After 60 months,  
20 all eligible patients were submitted to DUS follow-up. Intima-media thickness (IMT) was extracted  
21 offline at the following locations ICA distal the CB; CB; distal end of the common carotid artery  
22 (CCA), i.e., the flow divider (FD); CCA at 1cm and 2cm below the distal end of the CCA (FD-1cm and  
23 FD-2cm, respectively) (Table II). No symptoms of cerebrovascular ischemia secondary to  
24 restenosis were observed in any patient during the follow-up period.

## 25 26 **From acquisition of clinical images to 3D model reconstruction.**

27 MRI acquisitions were performed within a month after surgery with a Siemens 1.5T Avanto MR  
28 scanner with the following sequences and planes: Turbo Spin Echo T1 weighted axial (TR 7.50, TE  
29 8.9, FA 144, slice 4 mm, matrix 320 224 pixels); True Fisp single shot axial (TR 873.94, TE 1.36, FA

1 80, slice 4 mm, matrix 256 256 pixels) and coronal (TR 1781.93, TE 1.4, FA 72, slice 3 mm, matrix  
2 256 256 pixels) images; Turboflash 2D retrospectively electrocardiographically-gated axial  
3 images (TR 46.35, TE 1.3, FA 70, slice 6 mm, matrix 272 245 pixels).

4 From the acquired set of images, the 3D geometry of the carotid bifurcations was reconstructed  
5 using the Vascular Modeling Toolkit software (VMTK, [www.vmtk.org](http://www.vmtk.org)), as detailed elsewhere.<sup>19</sup>

6

### 7 **Computational Fluid Dynamics.**

8 Blood was modelled as an incompressible homogeneous Newtonian fluid, under laminar and rigid  
9 wall assumptions. Technically, the governing equations of fluid motion were numerically solved  
10 in meshes made of tetrahedral volumetric elements, using of P1 bubble-P1 finite elements and the  
11 library LifeV (<http://www.lifev.org>). In all cases, mesh size was set equal to about 0.2 cm after a  
12 mesh refinement study.<sup>19</sup> Patient-specific flow rate waveforms were extracted from echo-color  
13 Doppler at the CCA and ICA and imposed as boundary conditions in the numerical simulations.<sup>19</sup>  
14 From the instantaneous WSS distribution at the luminal surface, two WSS-based descriptors were  
15 calculated, i.e. the time-averaged WSS (TAWSS), and the oscillatory shear index (OSI).<sup>14, 20</sup> These  
16 hemodynamic descriptors quantify the occurrence of low and oscillatory shear stress,  
17 respectively, at the luminal surface.

18 For disturbed shear quantification, each carotid bifurcation was split in its constituent branches  
19 (i.e., CCA, ICA and external carotid artery, ECA), as outlined in previous studies.<sup>16</sup> To delimit the  
20 bifurcation region, the models were automatically clipped at sections located at 3, 5 and 2 radii  
21 along the CCA, ICA and ECA length, respectively (CCA3, ICA5 and ECA2) (Fig. 1A). Data from all  
22 cases were pooled to identify the 20<sup>th</sup> percentile value of TAWSS, and 80<sup>th</sup> percentile values of OSI,  
23 to determine thresholds for disturbed shear. The burden of disturbed WSS was quantified by the  
24 surface area exposed to OSI above (TAWSS, below) the corresponding threshold value, and  
25 divided by the model surface area.<sup>20</sup> These hemodynamic descriptors are denoted Low Shear Area  
26 (LSA) and Oscillatory Shear Area (OSA).

27

28

29

## 1 **Geometric analysis**

2 The analysis of the carotid bifurcation geometry was based on the vessel centerline, considered  
3 here the main geometric attribute of a vessel. Technically, the centerline was defined as the locus  
4 of the centers of the maximal inscribed spheres along the vessel itself.<sup>21</sup> Centerlines were  
5 calculated automatically as a set of discrete 3D points, which was used as input to obtain an  
6 analytical representation through 3D free-knots regression splines.<sup>22-23</sup>

7 Geometric descriptors previously demonstrated to be capable of predicting the underlying  
8 “disturbed” hemodynamics<sup>16-17</sup> were calculated automatically. These descriptors quantify the  
9 bifurcation flare (i.e., the expansion), and the tortuosity of the CCA proximal to the bifurcation.<sup>17</sup>  
10 Physically, a large expansion at the bifurcation promotes flow separation and in general flow  
11 disturbances,<sup>17</sup> that however can be limited by a curved or tortuous upstream tract thanks to the  
12 beneficial stabilizing effect of helical flow.<sup>23-24</sup> In detail, two descriptors quantifying flare were  
13 calculated. The first one, FlareA, was defined as the ratio between the maximum cross-sectional  
14 area at the CCA branch proximal to the flow divider ( $CCA_{max}$ ) and the CCA3 area, to measure the  
15 expansion of the CB with respect to the CCA (Figure 1A). The second flare descriptor (FlareR) was  
16 defined as half the difference between the two major axes of  $CCA_{max}$  and CCA3 ( $L_{max}$  and  $L_3$ ,  
17 respectively), divided by the distance between the two planes, to take into account the abruptness  
18 of the expansion (Fig. 1B).

19 Focusing on the quantification of tortuosity, the CCA centerline was split at the so-called “inflection  
20 point”, i.e. the point proximal to the flow divider where the typically sigmoidal-shaped CCA-ICA  
21 centerline changes concavity, and at the CCA3 centerline point (Fig. 1C). The first tortuosity  
22 descriptor, named Tort3D, was defined as  $L/D-1$ ,<sup>16</sup> where  $L$  is the curvilinear distance between  
23 the two points and  $D$  is the Euclidean distance between them (Fig. 1C). The second tortuosity  
24 descriptor (Tort2D) quantify the planar tortuosity of the CCA.<sup>17</sup> The centerline between CCA3 and  
25 the inflection point was projected onto a plane fitting the centerline segment with a least square  
26 minimization method. Tort2D was then calculated applying the definition of tortuosity to the  
27 projected centerline segment (Fig. 1D).

28

29

## 1 **Choice of geometric descriptors and comparison with follow-up clinical data**

2 The relationship between burden of disturbed hemodynamics and the combination of flare and  
3 tortuosity descriptors were quantified by multiple linear regression analysis. The quality of the  
4 regression was evaluated with the coefficient of determination  $R^2$ , adjusted by the number of  
5 independent predictors (equal to 2). The relative contribution of the predictors was determined  
6 from the standardized regression coefficients  $\beta$ . Successively, hemodynamic and geometric  
7 descriptors correlated with LSA or OSA were used to stratify the patients in tertiles to define three  
8 classes of “hemodynamic restenosis risk” and “geometric restenosis risk”. Through such  
9 stratification, the ability of the hemodynamic and geometric analysis to successfully identify  
10 patient clinical presentation at 60 months follow-up was tested. To compare the risk stratifications  
11 with the clinical outcomes at 60 months, maximum IMT values were likewise ranked in three  
12 classes.

## 14 **RESULTS**

### 16 **Analysis of Geometry, Hemodynamics and their relationship**

17 The values of flare and tortuosity descriptors for PG and PC groups are reported in Table III. As an  
18 average, PG cases presented higher values than PC of both FlareA ( $2.60 \pm 1.42$  vs.  $1.33 \pm 0.10$ ) and  
19 FlareR ( $0.23 \pm 0.11$  vs.  $0.16 \pm 0.03$ ). This is not unexpected as the inserted PG substitutes a portion  
20 of the endarterectomized wall, which is removed in PC. Conversely, PG and PC groups presented  
21 more similar values for Tort2D ( $0.031 \pm 0.023$  vs.  $0.042 \pm 0.019$ , respectively) and Curv2D  
22 ( $0.070 \pm 0.040$  vs.  $0.070 \pm 0.022$ , respectively).

23 Visualizations of WSS-based hemodynamic descriptors allow to observe that LSA and OSA are  
24 mostly localized at the carotid bulb in correspondence of the expansion. The quantitative analysis  
25 summarized by the bar diagrams (right panel) highlights that PG patients exhibit larger average  
26 values of LSA and OSA than PC patients (Fig. 2), confirming previous reports of more unfavorable  
27 hemodynamic conditions establishing in PG than PC subjects.<sup>25-26</sup> The interaction between the  
28 combination of flare and tortuosity vs. disturbed hemodynamics was investigated by performing  
29 multiple linear regressions over the 13 cases, with LSA or OSA as dependent variables and flare

1 and tortuosity descriptors as independent variables (Table III). Notwithstanding the small sample  
2 size, a significant direct relationship emerged between flare descriptors and LSA, as indicated by  
3 the statistical significant  $R^2$  and standardized correlation coefficients  $\beta$  ( $P < 0.05$ ) but not OSA  
4 ( $P > 0.05$ ) (Table IV).

5

## 6 **Restenosis risk assessment and comparison with clinical outcomes**

7 By virtue of the link with disturbed hemodynamics, emerged from the regression analysis, FlareA  
8 was considered for restenosis risk stratification (FlareR is not considered in this section for the  
9 sake of synthesis). The 13 cases were ranked in three classes using lower and upper FlareA  
10 distribution tertiles, defining *high*, *intermediate*, and *low* “geometric restenosis risk”. Furthermore,  
11 LSA and OSA distribution tertiles were similarly used to evaluate the “hemodynamic restenosis  
12 risk” (Fig. 3). Maximum IMT values were likewise ranked in three classes when the follow-up data  
13 were available. From the ranking, shown in Figure 3, it is evident that the high geometric and  
14 hemodynamic risk associated to PG1 and PG2 was reflected by high values of maximum IMT.  
15 Moreover, FlareA and LSA correctly classified 7 cases out of the 11 patients who survived during  
16 follow-up. OSA correctly classified 6 cases out of 11.

17 At 60 months, DUS showed the presence of an after CEA restenosis  $>70\%$  in PG1, and  $>50\%$  in PG2  
18 (reminding that belong to the same case) (Fig. 4 a-b) that was confirmed by MRA and intra-  
19 operatory arteriography (Fig. 4 c-d). Moreover, a clear correspondence emerged between the area  
20 exposed to low and oscillatory WSS, shown through contours of TAWSS and OSI (Fig. 4 e-f), and  
21 the restenosis location (as indicated by the arrows).

22 Clinical DUS measurements of the maximum IMT values at the end of the 60 months follow-up  
23 period are all reported in Table II. Moreover, a clear correspondence emerged between the area  
24 exposed to low and oscillatory WSS, shown through contours of TAWSS and OSI (Fig. 4 e-f), and  
25 the restenosis location (as indicated by the arrows). A marked IMT (maximum IMT equal to 2.6  
26 mm, Table II) was observed at follow-up for PG3, which was characterized by a high geometric  
27 restenosis risk, high LSA risk but intermediate OSA risk. Marked IMT was observed at follow-up  
28 also for PG6 (maximum IMT equal to 2.1 mm, Table II), classified as intermediate restenosis risk  
29 by its FlareA value and LSA, but high risk by OSA. Moreover, a focal restenosis process at the FD at

1 follow-up was observed for PC2, classified as intermediate restenosis risk by its FlareA value and  
2 LSA, and high risk by OSA. In all the remaining cases (PG5, PG7, PG8, PG9, PC1, PC3, PC4), we  
3 observed a moderate IMT (Table II).

4 Morphological DUS observation of the endoarterectomized regions were reported for all cases  
5 together with the TAWSS and OSI distributions at the luminal surface to appreciate the co-  
6 localization between disturbed hemodynamics and DUS observations of myointimal thickening or  
7 new atheroma development (Fig. 5). Generally, in all cases a remarkable co-localization was  
8 observed with LSA (ten out of eleven cases), while OSA results appeared weaker (six out of eleven  
9 cases) (Table V).

10

## 11 **DISCUSSION**

12

13 Severe late restenosis after CEA constitutes a major problem. Nonetheless, mechanisms for the  
14 development of carotid restenosis after CEA are still being defined. Among the involved risk  
15 factors, the establishment of flow disturbances at the bifurcation has been often interpreted by  
16 the surgeons as an harbinger of potential complications after CEA.<sup>27</sup>

17 To the best of our knowledge, this is the first study that (1) linked disturbed hemodynamics after  
18 CEA to verified cases of late restenosis, and (2) explored the clinical translation of such a link  
19 through surrogate geometric predictors of disturbed hemodynamics. According to this study,  
20 hemodynamic and geometric analyses hold potential for the stratification of patients at risk for  
21 development of late restenosis. In particular the investigated descriptors LSA, OSA and FlareA  
22 resulted associated to the clinical outcomes at 60 months follow-up. Misclassifications were  
23 limited to contiguous categories and regarded all descriptors for PG9 and PC4, while PC2 was  
24 correctly classified by OSA only and PG7 by FlareA only (Figure 3). Moreover, geometric restenosis  
25 risk was overestimated for case PG5 (i.e., risk was represented in a conservative way), but the  
26 hemodynamic restenosis risk for this case was correctly estimated. Interestingly, the PG in case  
27 PG5 is placed distally to the CB, as the pre-CEA blockage was localized in the ICA. As a consequence,  
28 its “intermediate-risk” FlareA value was relative to the native CB, which was exposed to a low  
29 amount of disturbed WSS, and it did not develop, neither primary atherosclerotic lesion nor

1 restenosis. Furthermore, the present CFD analysis based on LSA and OSA quantification allowed  
2 us also to predict with a good approximation the location of maximum IMT, regardless of its  
3 severity. The differences in the association between clinical outcomes and LSA or OSA suggest  
4 different vascular responses to low vs. oscillatory WSS.<sup>28</sup>

5 Several investigations focused at the hemodynamic alterations consequent to variations of carotid  
6 bifurcation geometry after CEA. Kamenskiy et al. observed wider areas of high OSI as a  
7 consequence of the abrupt diameter's transition from PG level to the native artery after PG  
8 insertion, consistently with the idea of flare promoting disturbed WSS.<sup>29</sup> Harloff et al. investigating  
9 carotid bifurcation of previously high-grade ICA stenosis, reported that eversion CEA tends to  
10 restore WSS to physiological values.<sup>30</sup> Domanin et al. observed higher values of OSI in patients  
11 submitted to CEA when PG was inserted with respect to PC, both in obliged and selective use of PG  
12 based on the measures of the ICA or the proximal localization of the plaque.<sup>25</sup> The opposite  
13 scenarios, explored by virtually adding or removing the PG, did not highlight disadvantages for the  
14 PC choice from an hemodynamic point of view.<sup>26</sup>

15 Surrogate markers for disturbed WSS have been proposed based on specific geometric attributes  
16 of the carotid artery, by virtue of their influence on local flow patterns.<sup>16, 31-33</sup> Bijari et al.  
17 demonstrated that flare and proximal CCA curvature are independent predictors of LSA and OSA<sup>33</sup>  
18 and wall thickness at the carotid bulb.<sup>17</sup> Archie observed that PG insertion resulted in CB  
19 geometric modifications with respect to the pre-CEA geometry, with an increase of the CB length,  
20 and a change of CB shape from elliptical to round.<sup>34</sup> Here, flare emerged as significant predictor of  
21 exposure to disturbed hemodynamics, recapitulating the detrimental effect of flare in promoting  
22 disturbed WSS.<sup>16, 33</sup> These findings are widened by the association between flare and long-term  
23 clinical outcomes, supporting that the introduction of a large and sudden expansion<sup>4</sup> should be  
24 avoided. In other words, an artificial enlargement of the carotid bifurcation would increase the  
25 amount of disturbed flow, potentially leading to abnormal responses of the endarterectomised  
26 arterial wall. This is particularly true in PG arteriotomy repair strategies. Furthermore, the  
27 statistical analysis revealed an inverse relative contribution of tortuosity to disturbed  
28 hemodynamics (as indicated by the negative standardized coefficients in Table IV), although not

1 significant. This summarized the beneficial effect of inlet tortuosity in mitigating WSS  
2 disturbances.<sup>23-24</sup>

3 It is worth noting that previous studies demonstrated the reproducibility of the geometric  
4 characterization of the carotid bifurcation, <sup>24</sup> that was performed here automatically. Therefore,  
5 the quantitative geometric characterization described here could be easily and robustly obtained  
6 from imaging data, and employed at a large scale for explorative studies, clinical trials and  
7 ultimately clinical routine. In this sense, FlareR was considered here based upon the idea that  
8 FlareR can be measured from one 2D planar view, and thereby it represents an easy to measure  
9 geometric indicator. The robustness of our findings was checked repeating the geometric  
10 restenosis risk stratification using FlareR instead of FlareA: comparable results were obtained in  
11 terms of LSA and OSA prediction and restenosis risk stratification.

12

### 13 **Limitations and future developments**

14 Limitations are related to the small sample size, although sufficient for statistical significant  
15 correlations to emerge, to the lack of randomization, and to the absence of any analysis of biologic  
16 factors potentially involved in the physio-pathologic mechanism of restenosis. Therefore, the  
17 proposed diagnostic criteria will need to be validated in a prospective trial. Moreover, in general  
18 computational hemodynamics suffers from uncertainties (e.g., reconstruction errors), and  
19 assumptions (e.g., Newtonian viscosity, rigid walls, as widely discussed elsewhere <sup>15</sup>), that might  
20 influence the relationships described in the present study. Additionally, no information about the  
21 extension of the region subject to CEA surgical intervention (either with PG or PC) can be extracted  
22 from the imaging data.

23

### 24 **CONCLUSIONS**

25

26 One main challenge for vascular surgeons is the prediction of the long-term outcomes of surgery.  
27 The question of the proper use of PG in carotid surgery has been going for many years and  
28 concerns about its use still persist.

1 In this still unclear scenario, hemodynamics plays an important role in determining conditions for  
2 the restenosis initiation processes to occur. In this direction, CFD has revealed to be an effective  
3 tool to predict such conditions. Moreover, as arterial geometry shapes the flow, the analysis of  
4 geometric descriptors could be a useful surrogate to predict, with a good accuracy, flow  
5 disturbances and their consequences at the carotid bifurcation in the clinical practice. In this  
6 sense, geometric analysis based on flare can be obtained by DUS or radiological imaging during  
7 the preoperative clinical assessment in a convenient, fast and relatively easy way, allowing to  
8 provide useful indications about the best closure technique to adopt on a case by case basis in a  
9 time frame compatible with clinical procedures.

10

11 **Disclosures:** None

12

## 1 REFERENCES

2

- 3 1. Rerkasem K, Rothwell PM. Systematic review of randomized controlled trials of patch  
4 angioplasty versus primary closure and different types of patch materials during carotid  
5 endarterectomy. *Asian J Surg.* 2011;34:32-40.
- 6 2. Kumar R, Batchelder A, Saratzis A, AbuRahma AF, Ringleb P, Lal BK et al. Restenosis after  
7 Carotid Interventions and Its Relationship with Recurrent Ipsilateral Stroke: A Systematic  
8 Review and Meta-analysis. *Eur J Vasc Endovasc Surg.* 2017;53:766-75.
- 9 3. Frericks H, Kievit J, van Baalen JM, van Bockel JH. Carotid recurrent stenosis and risk of  
10 ipsilateral stroke: a systematic review of the literature. *Stroke.* 1998;29:244-50.
- 11 4. Imparato AM. The role of patch angioplasty after carotid endarterectomy. *J Vasc Surg.*  
12 1988;7:715-6.
- 13 5. Hellings WE, Moll FL, de Vries JP, de Bruin P, de Kleijn DP, Pasterkamp G. Histological  
14 characterization of restenotic carotid plaques in relation to recurrence interval and clinical  
15 presentation: a cohort study. *Stroke.* 2008;39:1029-32.
- 16 6. Brott TG, Halperin JL, Abbara S, Bacharach JM, Barr JD, Bush RL et al. 2011  
17 ASA/ACCF/AHA/AANN/AANS/ACR/ASNR/CNS/SAIP/SCAI/SIR/SNIS/SVM/SVS guideline  
18 on the management of patients with extracranial carotid and vertebral artery disease.  
19 *Circulation.* 2011;124:e54-130.
- 20 7. Naylor AR, Ricco JB, de Borst GJ, Debus S, de Haro J, Halliday A, et al. Management of  
21 Atherosclerotic Carotid and Vertebral Artery Disease: 2017 Clinical Practice Guidelines of  
22 the European Society for Vascular Surgery (ESVS). *Eur J Vasc Surg.* 2018 ; 55:3-81.
- 23 8. Zenonos G, Lin N, Kim A, Kim JE, Governale L, Friedlander RM. Carotid endarterectomy with  
24 primary closure: analysis of outcomes and review of literatures. *Neurosurgery.*  
25 2012;70:646-55.
- 26 9. Heyer EJ, Sharma R, Rampersad A, et al. A controlled prospective study of  
27 neuropsychological dysfunction following carotid endarterectomy. *Arch*  
28 *Neurol.*2002;59:217-22.

- 1 10. Abdelhamid MF, Wall ML, Vohra RK. Carotid Artery Pseudoaneurysm After Carotid  
2 Endarterectomy: Case Series and a Review of the Literature. *Vascular and Endovascular*  
3 *Surgery* 2009;43:571-7.
- 4 11. Ouriel K, Green RM. Clinical and technical factors influencing recurrent carotid stenosis and  
5 occlusion after endarterectomy. *J Vasc Surg* 1987;5:702-6.
- 6 12. Pasterkamp G, de Kleijn DPV, Borst C. Arterial remodeling in atherosclerosis, restenosis and  
7 after alteration of blood flow: potential mechanisms and clinical implications. *Cardiov Res*  
8 2000;45:843-52.
- 9 13. Morbiducci U, Kok AM, Kwak BR, Stone PH, Steinman DA, Wentzel JJ. Atherosclerosis at  
10 arterial bifurcations: evidence for the role of hemodynamics and geometry. 2016;115:484-  
11 92.
- 12 14. Ku DN, Giddens DP, Zarins CK, Glagov S. Pulsatile flow and atherosclerosis in the human  
13 carotid bifurcation. Positive correlation between plaque location and low oscillating shear  
14 stress. *Arteriosclerosis* 1985;5:293-302.
- 15 15. Taylor CA, Steinman DA. Image-based modeling of blood flow and vessel wall dynamics:  
16 applications, methods and future directions. *Ann Biomed Eng* 2010; 38:1188-203.
- 17 16. Lee SW, Antiga L, Spence JD, Steinman DA. Geometry of the carotid bifurcation predicts its  
18 exposure to disturbed flow. *Stroke*. 2008;39:2341-7
- 19 17. Bijari PB, Antiga, Gallo D, Wasserman BA, Steinman DA. Improved Prediction of Disturbed  
20 Flow via Hemodynamically-Inspired Geometric Variables. *J Biomech*. 2012;45:1632-7.
- 21 18. AbuRahma AF, Stone P, Deem S, Dean LS, Keiffer T, Deem E. Proposed duplex velocity criteria  
22 for carotid restenosis following carotid endarterectomy with patch closure. *J Vasc Surg*.  
23 2009;50:286-91.
- 24 19. Guerciotti B, Vergara C, Azzimonti L, Forzenigo L, Buora A., Biondetti P et al. Computational  
25 study of the fluid-dynamics in carotids before and after endarterectomy. *Journal of*  
26 *Biomechanics*. 2016;49:26-38.
- 27 20. Gallo D, Steinman DA, Morbiducci U. Insights into the co-localization of magnitude-based  
28 versus direction-based indicators of disturbed shear at the carotid bifurcation. *J Biomech*.  
29 2016;49:2413-9.

- 1 21. Antiga L, Piccinelli M, Botti L, Ene-Iordache B, Remuzzi A, Steinman DA. An image-based  
2 framework for patient-specific computational hemodynamics. *Med Biol Eng Comput* 2008;  
3 46:1097-112
- 4 22. Sangalli LM, Secchi P, Vantini S, Veneziani A. Efficient estimation of three-dimensional curves  
5 and their derivatives by free-knot regression splines, applied to the analysis of inner carotid  
6 artery centrelines. *Appl Statist* 2009;58:286-306.
- 7 23. Gallo D, Steinman DA, Morbiducci U. An insight into the mechanistic role of the common  
8 carotid artery on the hemodynamics at the carotid bifurcation. *Ann Biomed Eng* 2015; 43:68-  
9 81.
- 10 24. Gallo D, Steinman DA, Bijari PB, Morbiducci U. Helical flow in carotid bifurcation as surrogate  
11 marker of exposure to disturbed shear. *J Biomech* 2012;45:2398-404.
- 12 25. Domanin M, Buora A, Scardulla F, Guerciotti B, Forzenigo L, Biondetti P et al. Computational  
13 fluid-dynamic analysis after carotid endarterectomy: patch graft versus direct suture  
14 closure. *Ann Vasc Surg* 2017;44:325-35.
- 15 26. Domanin M, Bissacco D, Le Van D, Vergara C. Computational fluid dynamic comparison  
16 between patch-based and primary closure techniques after carotid endarterectomy. *J Vasc*  
17 *Surg* 2018;67:887-97.
- 18 27. Bandyk DF, Kaebnick HW, Adams MB, Towne JB. Turbulence occurring after carotid  
19 bifurcation endarterectomy: a harbinger of residual and recurrent carotid stenosis. *J Vasc*  
20 *Surg.* 1988;7:261-74.
- 21 28. Timmins LH, Molony DS, Eshtehardi P, McDaniel MC, Oshinski JN, Giddens DP, Samady H.  
22 Oscillatory wall shear stress is a dominant flow characteristic affecting lesion progression  
23 patterns and plaque vulnerability in patients with coronary artery disease. *J R Soc Interface.*  
24 2017;14: 20160972;
- 25 29. Kamenskiy AV, Pipinos II, Dzenis YA, Gupta PK, Jaffar Kazmi SA, MacTaggart JN. A  
26 mathematical evaluation of hemodynamic parameters following carotid eversion and  
27 conventional patch angioplasty. *Am J Physiol Heart Circ Physiol.* 2013;305:716-24.

- 1 30. Harloff A, Berg S, Barker AJ, Schöllhorn J, Schumacher M, Weiller C et al. Wall shear stress  
2 distribution at the carotid bifurcation: influence of eversion carotid endarterectomy. *Eur*  
3 *Radiol.* 2013;23:3361–9.
- 4 31. Sitzer M, Puac D, Buehler A, Steckel DA, von Kegler S, Markus HS et al. Internal carotid artery  
5 angle of origin: a novel risk factor for early carotid atherosclerosis. *Stroke.* 2003;34:950–55.
- 6 32. Phan TG, Beare RJ, Jolley D, Das G, Ren M, Wong K, et al. Carotid artery anatomy and geometry  
7 as risk factors for carotid atherosclerotic disease. *Stroke.* 2012;43:1596–601.
- 8 33. Bijari PB, Wasserman BA, Steinman DA. Carotid bifurcation geometry is an independent  
9 predictor of early wall thickening at the carotid bulb. *Stroke.* 2014;45:473-8.
- 10 34. Archie JP Jr. Geometric dimension changes with carotid endarterectomy reconstruction. *J*  
11 *Vasc Surg.* 1997;25:488-98.

12

13

14

15

16

17

18

19

20

21

22

23

24

25

26

27

28

29

1 **FIGURES LEGENDS**

2

3 **Fig.1**

4 A) CCAMax and CCA3 sections, whose areas define FlareA, are shown in red. CCAMax is normal to  
5 the average of the internal (ICA) and external carotid artery (ECA) centerlines. B) FlareR was  
6 calculated as half the difference between CCA3 and CCAMax major axes (Lmax and L3,  
7 respectively), divided by the distance between the sections, indicated as L in the figure. C) The  
8 centerline segment between the CCA3 centerline point and the inflection point was used to  
9 calculate Tort3D as  $L/D-1$ , where L is the curvilinear distance between the two points and D is the  
10 Euclidean distance between them. D) The centerline segment between CCA3 and inflection point  
11 was projected to a least-squares plane. The projected segment on the fitting plane defines Tort2D  
12 as  $L/D-1$ .

13

14 **Fig. 2**

15 Exposure to disturbed WSS in the 13 models (PG patch graft, PC primary closure). The bifurcation  
16 region is delimited by sections CCA3, ICA5 and ECA2 and indicated by black lines in the figure.  
17 Quantitative analysis of LSA and OSA in the bifurcation region for the two groups is visualized with  
18 bar diagrams in terms of mean  $\pm$  standard deviation. Top row: exposure to low WSS as expressed  
19 by LSA. Red and black areas denote TAWSS values below respectively the 20th and 10th percentile  
20 of the pooled TAWSS distribution on all models. Bottom row: exposure to highly oscillatory WSS,  
21 as expressed by OSA. Red and black areas denote OSI values above respectively the 80th and 90th  
22 percentile of the pooled OSI distribution on all models.

23

24 **Fig. 3**

25 Comparison between restenosis risk assessed by hemodynamic (LSA and OSA) and geometric  
26 (FlareA) descriptors and maximum IMT, measured through clinical ultrasound imaging. Bar color  
27 represents the restenosis risk stratification: red, high risk; orange, intermediate risk; green, low  
28 risk. Top row, left panel: Restenosis risk stratification based on LSA. Top row, right panel:  
29 Restenosis risk stratification based on OSA. Bottom row, left panel: Restenosis risk stratification

1 based on FlareA. Bottom row, right panel: Maximum IMT, expressed in mm, shows a good  
2 correspondence with LSA and FlareA data. Patients PG4 and PG8 died at three years from CEA  
3 surgery for unrelated causes, thus no follow-up data are present.

4

5 Fig. 4

6 Clinical evidences of restenosis for PG1 and PG2 (note that the carotids belong to the same  
7 patient). Panel a) and b): DUS analyses for PG1 and PG2 respectively indicated a severe restenosis  
8 and  $PSV > 130 \text{ cm/s}$ . Panel c) MRA examinations confirming the restenosis in both carotids. Panel  
9 d): Intra-operative arteriography. Panel e): contours of TAWSS (in Pa) and OSI for PG1  
10 highlighted that the region where restenosis occurred was characterized by low and oscillatory  
11 WSS, as underlined by the arrow.

12

13 Fig. 5

14 Contour maps of low and oscillatory WSS, as indicated by TAWSS (Pa) and OSI, are shown together  
15 with follow-up DUS images at 60 months, showing carotid IMT. In general, there is correspondence  
16 between low and oscillatory WSS regions and maximum IMT regions.

17

18

19

20

21

22

23

24

25

26

27

28

29

1 **TABLES LEGENDS**

2

3 Table I.

4 Age, classification of sex (F female; M male), localization of the carotid blockage (CCA Common  
5 carotid artery; B Bulb; ICA Internal carotid artery; ECA external carotid artery), diameter  
6 measurements at CCA, B, ICA and ECA, and closure technique (PG Patch graft; PC Primary closure).

7

8 Table II.

9 Doppler ultrasound analysis of carotid after 60 months: Peak systolic velocity, end diastolic  
10 velocity, IMT measurements at the bifurcation division level (flow divider, FD), CCA at 2cm and  
11 1cm proximal to the FD (FD-2cm and FD-1cm), at the carotid bulb (CB), at the ICA downstream of  
12 the CB, and maximum IMT. , and correspondence between the localization of maximum IMT with  
13 LSA and OSA.

14

15 Table III.

16 Values of geometric descriptors: FlareA, FlareR, Tort3D and Tort2D.

17

18 Table IV.

19 Multiple regression between geometry vs hemodynamics.

20

21 Table V.

22 Correspondence between the localization

23

24

25

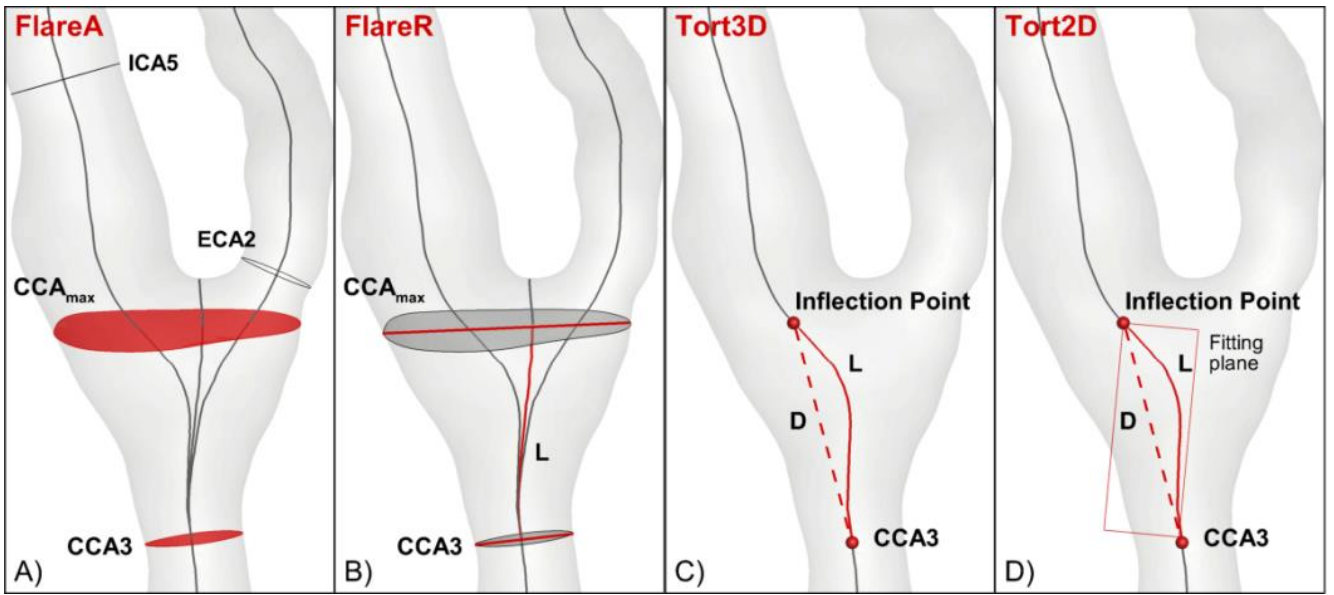
26

27

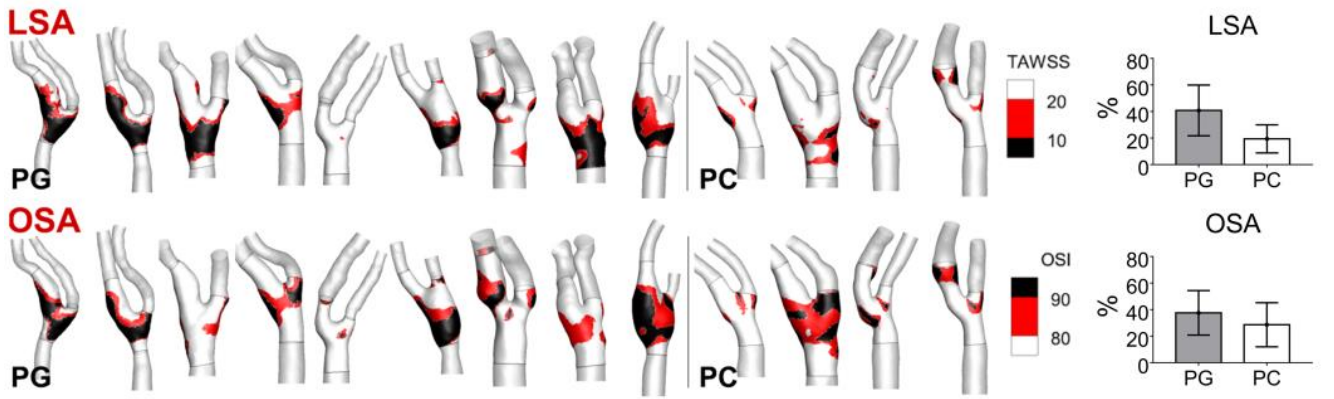
28

29

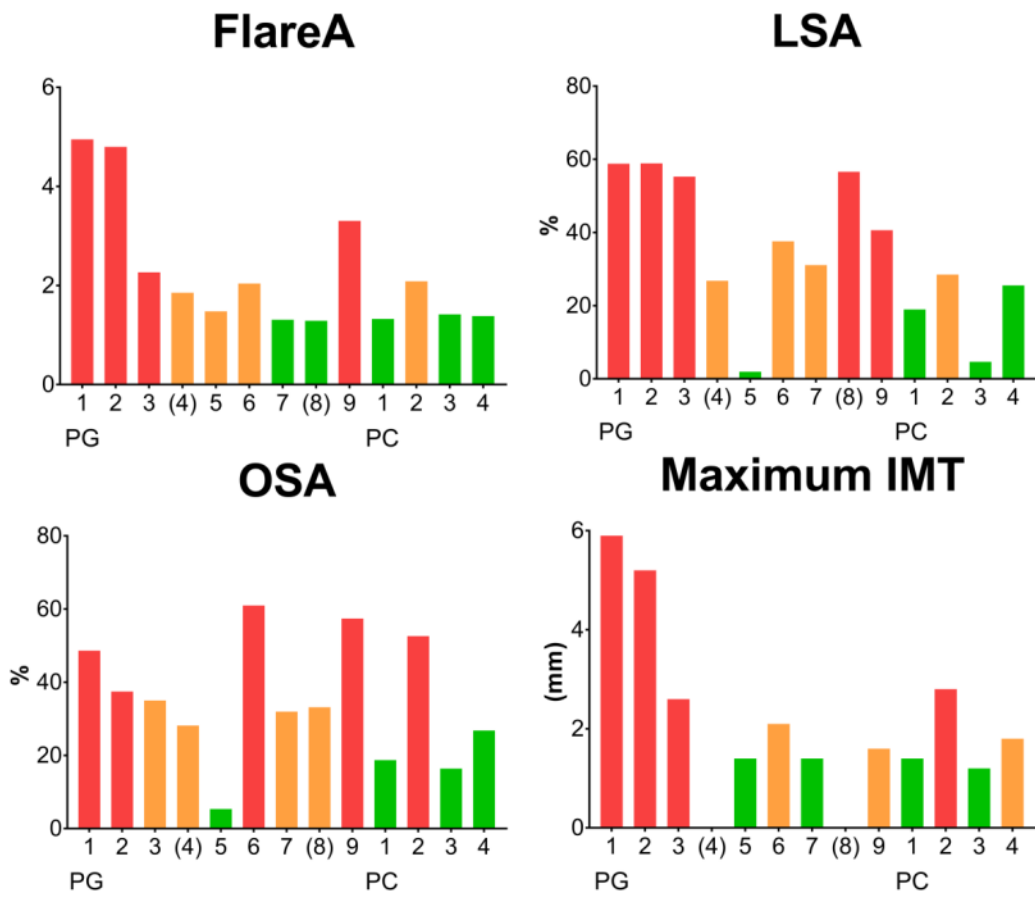
1 **Figure 1**



7 **Figure 2**

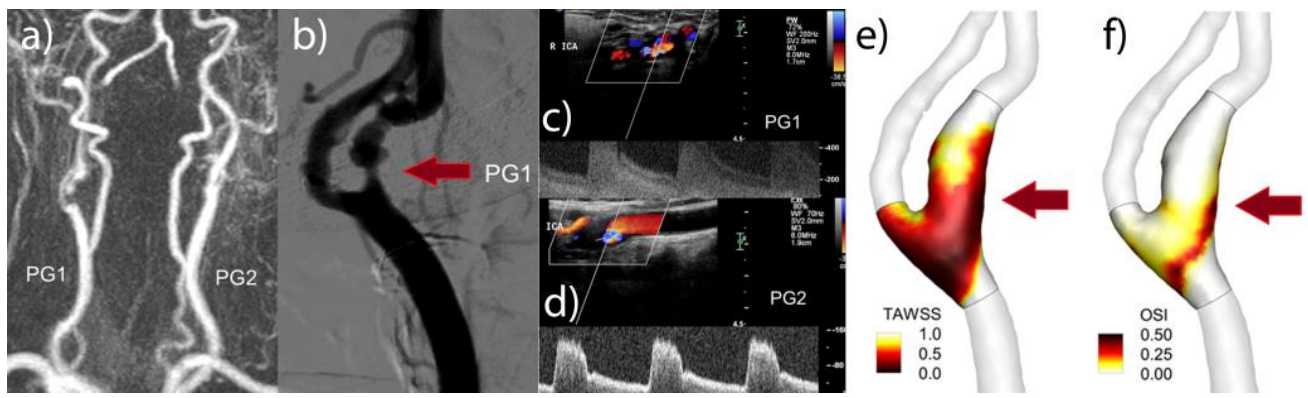


1 **Figure 3**



2  
3  
4  
5  
6  
7

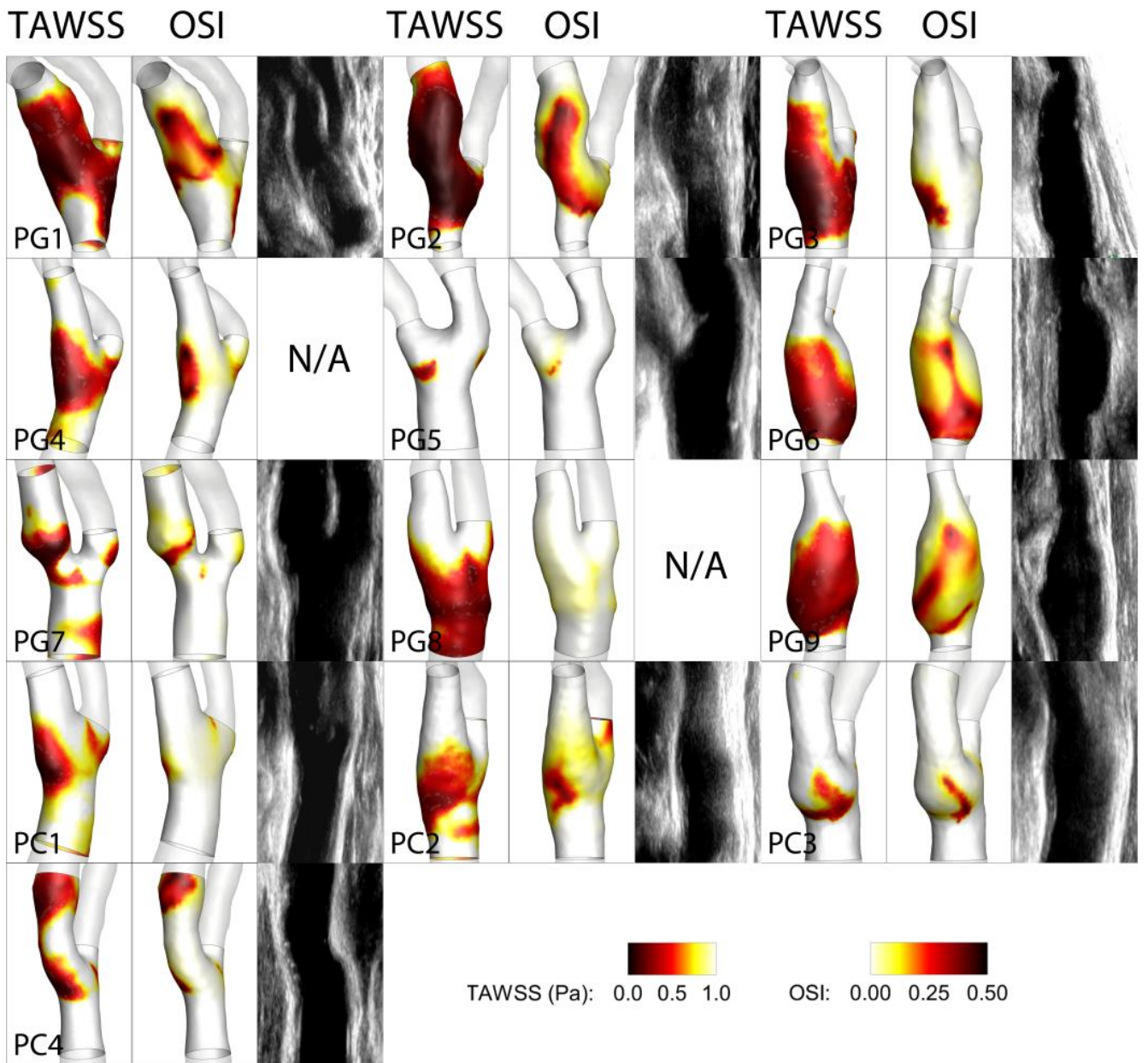
7 **Figure 4**



8

1 **Figure 5**

2



3

4

5

6

7

8

1 **Table I.**

2

Patient	Age (years)	Sex	Plaque Localization	CCA $\Phi$ (mm)	BULB $\Phi$ (mm)	ICA $\Phi$ (mm)	ECA $\Phi$ (mm)	Closure technique
PG1	65	F	CCA, B	6,00	6,00	5,00	3,80	PG
PG2	65	F	B	6,00	5,90	5,40	4,00	PG
PG3	81	F	B, ICA	6,80	5,40	4,20	3,50	PG
PG4	82	F	B, ICA	6,60	5,40	4,00	3,80	PG
PG5	72	M	ICA	6,69	4,83	4,50	3,97	PG
PG6	68	F	B	5,82	5,04	4,50	4,10	PG
PG7	71	F	B, ICA	6,00	6,00	4,90	3,26	PG
PG8	76	M	B	7,00	5,15	4,00	3,86	PG
PG9	67	M	B, ICA	6,33	6,20	4,80	2,40	PG
PC1	81	F	B, ICA	7,48	7,52	4,74	4,00	PC
PC2	79	M	B, ICA	6,17	7,00	5,00	3,25	PC
PC3	79	M	CCA, B, ICA	8,00	8,80	7,00	5,00	PC
PC4	61	M	B	6,88	7,62	6,60	5,40	PC

3

1 **Table II.**

2

Patient	Peak systolic velocity (cm/s)	End diastolic velocity (cm/s)	Degree of restenosis (%)	IMT @ FD-2cm (mm)	IMT @ FD-1cm (mm)	IMT @ FD (mm)	IMT @ CB (mm)	IMT @ ICA (mm)	Max IMT (mm)
PG1	> 400	200	>70	0.8	1.8	1.9	5.9	2.0	5.9
PG2	160	90	>50	0.8	0.7	2.1	4.8	0.9	5.2
PG3	80	40	<30	1.0	1.0	2.6	1.0	1.4	2.6
PG4	N/A	N/A	N/A	N/A	N/A	N/A	N/A	N/A	N/A
PG5	60	30	<30	1.0	1.3	1.3	1.4	0.7	1.4
PG6	80	40	<30	2.1	1.0	1.0	1.6	0.9	2.1
PG7	50	30	<30	0.6	0.9	0.9	1.4	1.0	1.4
PG8	N/A	N/A	N/A	N/A	N/A	N/A	N/A	N/A	N/A
PG9	90	40	<30	1.0	1.6	1.0	0.8	1.3	1.6
PC1	90	35	<30	0.9	0.9	0.9	0.9	0.9	1.4
PC2	70	35	<30	0.9	1.4	2.8	1.3	0.8	2.8
PC3	80	40	<30	0.7	0.8	0.9	0.9	0.6	1.2
PC4	60	40	<30	0.6	0.7	1.8	0.8	0.6	1.8

3

4

5

6

7

8

1 **Table III**

2

3

	<b>FLARE DESCRIPTOR</b>		<b>TORTUOSITY DESCRIPTOR</b>	
<b>Patient</b>	<b>FlareA</b>	<b>FlareR</b>	<b>Tort3D</b>	<b>Tort2D</b>
PG1	4.952	0.455	0.067	0.064
PG2	4.800	0.385	0.052	0.044
PG3	2.266	0.188	0.034	0.022
PG4	1.855	0.175	0.033	0.032
PG5	1.437	0.132	0.043	0.039
PG6	2.047	0.153	0.053	0.046
PG7	1.310	0.181	0.045	0.043
PG8	1.455	0.148	0.028	0.026
PG9	3.305	0.253	0.02	0.014
PC1	1.320	0.180	0.021	0.019
PC2	1.197	0.178	0.034	0.032
PC3	1.418	0.115	0.061	0.059
PC4	1.383	0.171	0.037	0.035

4

5

1 **Table IV.**

2

	LSA			OSA		
	Adjusted $R^2$	$\beta$ Flare	$\beta$ Tortuosity	Adjusted $R^2$	$\beta$ Flare	$\beta$ Tortuosity
FlareA, Tort3D	<b>0.3586*</b>	<b>0.7437*</b>	-0.2551	0.1323	0.5737	-0.1995
FlareA, Tort2D	<b>0.3840*</b>	<b>0.7307*</b>	-0.2894	0.1402	0.5586	-0.2102
FlareR, Tort3D	<b>0.3444*</b>	<b>0.7296*</b>	-0.2398	0.0167	0.4600	-0.1477
FlareR, Tort2D	<b>0.3881*</b>	<b>0.7395*</b>	-0.3096	0.0341	0.4668	-0.1929

3 \*  $P < 0.05$

4

5

6

7

8

9

10

11

12

13

14

15

1 **Table V.**

2

Patient	Localization maximum IMT/restenosis	LSA Co-localization	OSA Co-localization
PG1	B/ICA	High	High
PG2	B/ICA	High	High
PG3	CCA	High	High
PG4	N/A	N/A	N/A
PG5	CCA	High	Moderate
PG6	CCA	High	Moderate
PG7	B/ICA	Moderate	Moderate
PG8	N/A	N/A	N/A
PG9	CCA/B	High	Moderate
PC1	B	High	Low
PC2	CCA/B	High	High
PC3	B	High	High
PC4	B/ICA	High	High

3

4

5

## MOX Technical Reports, last issues

Dipartimento di Matematica  
Politecnico di Milano, Via Bonardi 9 - 20133 Milano (Italy)

- 37/2018** Bonaventura, L.; Della Rocca A.;  
*Convergence analysis of a cell centered finite volume diffusion operator on non-orthogonal polyhedral meshes*
- 36/2018** Agosti, A.; Ambrosi, D.; Turzi, S.  
*Strain energy storage and dissipation rate in active cell mechanics*
- 35/2018** Possenti, L.; Casagrande, G.; Di Gregorio, S.; Zunino, P.; Costantino, M.L.  
*Numerical simulations of the microvascular fluid balance with a non-linear model of the lymphatic system*
- 34/2018** Laurino, F.; Coclite, A.; Tiozzo, A.; Decuzzi, P.; Zunino, P.;  
*A multiscale computational approach for the interaction of functionalized nanoparticles with the microvasculature*
- 32/2018** Dal Santo, N.; Deparis, S.; Manzoni, A.; Quarteroni, A.  
*An algebraic least squares reduced basis method for the solution of nonaffinely parametrized Stokes equations*
- 31/2018** Quarteroni, A.  
*The role of statistics in the era of big data: A computational scientist' perspective*
- 30/2018** Ieva, F.; Palma, F.; Romo, J.  
*Bootstrap-based Inference for Dependence in Multivariate Functional Data*
- 29/2018** Manzoni, A; Bonomi, D.; Quarteroni, A.  
*Reduced order modeling for cardiac electrophysiology and mechanics: new methodologies, challenges & perspectives*
- 28/2018** Gerbi, A.; Dede', L.; Quarteroni, A.  
*Segregated algorithms for the numerical simulation of cardiac electromechanics in the left human ventricle*
- 26/2018** Vergara, C.; Zonca, S.  
*Extended Finite Elements method for fluid-structure interaction with an immersed thick non-linear structure*